Identification of the Transition States in the Inversion of 1,4-Benzodiazepines with the *Ab Initio* Replica Path Method

Yong-Sok Lee,*,† Victor W. Pike,‡ and Milan Hodoscek§,#

Center for Molecular Modeling, Division of Computational Bioscience, Center for Information Technology, National Institutes of Health, Building 12A, Room 2049, Bethesda, Maryland 20892, Molecular Imaging Branch, National Institute of Mental Health, National Institutes of Health, Building 10, Room B3C 346A, 10 Center Drive, Bethesda, Maryland 20892, National Heart, Lung and Blood Institute, National Institutes of Health, DHHS, Bethesda, Maryland 20892, National Institute of Chemistry, Ljubljana, Slovenia

Received: October 8, 2007; In Final Form: November 21, 2007

The inversion of four 1,4-benzodiazepines was investigated with the *ab initio* "replica path method" with density functional theory at the B3LYP/6-31G* level. The reaction path constructed with this method for the inversion provides an approximate transition state (TS) geometry, which, upon further TS optimization, leads to the TS geometry characterized by a single vibrational frequency. 1,4-Benzodiazepines lacking a 5-phenyl ring have a single reaction path for the inversion with C_s symmetry at the TS. In contrast, the inversion of benzodiazepines with a 5-phenyl ring, such as the peripheral benzodiazepine receptor ligand 4′-chlorodiazepam (Ro5-4864) and its N^1-desmethyl analog (Ro5-2752), can proceed through multiple reaction paths having a TS with or without C_s symmetry. Notably, the replica path method found a path connecting two asymmetric TSs of 4′-chlorodiazepam via a symmetrical TS, suggesting that these inversion paths can be readily crossed from one to another. The stabilization energies gained by 4′-chlorodiazepam and its N^1-desmethyl analog from the breaking of C_s symmetry at the TS were calculated to be 0.10 and 0.07 kcal/mol, respectively. The origin of the broken symmetry of C_s was traced to the coupling of the puckering of the diazepine ring with the rotation of the chlorophenyl ring. These results show the advantages of the replica path method for locating the TSs as well as for constructing the reaction paths for the inversion of 1,4-benzodiazepines.

1. Introduction

Analysis of structural modifications occurring upon binding of a ligand to a biomolecule and of any ensuing chemistry may require the transition state (TS) structure along reaction coordinates to be known. In drug development, knowledge of the TS geometry of a substrate for an enzyme is helpful when designing TS analogues that are known to bind generally more tightly than substrates to enzyme active sites.[1] Theoretical calculation may be the only viable method for obtaining the potential energy surface (PES) relevant to binding and ultimate chemistry.

A PES for a chemical process is typically constructed by carrying out geometry optimization coupled with a scan of a reaction coordinate. This coordinate can be defined, for example, as the distance between the two atoms undergoing bond breaking/forming or as the dihedral angle of the bond within a molecule that is primarily involved with a conformational change or isomerization of interest. From a PES, one could locate a TS, typically the highest-energy point on a reaction path. Once the TS is verified by a single imaginary vibrational frequency, the "intrinsic reaction coordinate" (IRC) method[2] can then be utilized to find the steepest-descent paths from the TS to both the initial and final geometries to construct the minimum energy path. With increases in computer speed and advances in TS search algorithms,[3,4] the geometry and energetics of the TS of small molecules undergoing reaction with a well-defined reaction coordinate can now be obtained at the *ab initio* level. Nonetheless, as the complexity of a molecule grows (*e.g.*, the number of rotatable bonds), it becomes increasingly difficult to locate the TS(s) by utilizing either a conventional scan method or one of the more sophisticated reaction path methods, because they often require prior knowledge of the TS geometry.

In this regard, a recently developed "replica path" (RPATH) method for elucidating the reaction mechanisms of enzymes has found its utility in locating a TS of interest, as exemplified in a recent study of the mechanism of chorismate mutase.[5] The RPATH calculation allows an approximate TS geometry to be found for a particular reaction or conformation through geometrical optimization at the *ab initio* level on intermediate structures lying between reactant and product in root-mean-square (rms) space. This RPATH method is currently implemented in CHARMM[6] interfaced with GAMESS,[7] Q-Chem,[8] and GAMESS-UK[9] *ab initio* programs for QM/MM calculations.

The RPATH method belongs to a class of string methods to determine the pathway on the PES between two or more different points.[10] Usually these points represent minima on the PES, which are relatively easy to obtain by standard methods, and are fixed during the pathway optimization. The pathway in the RPATH method is constructed by replicating a set of structures spanning, for example, reactant and product. The coordinates for each of these replicas, which are used to construct the initial pathway, can be obtained in different ways.

* Corresponding author. E-mail: Leeys@mail.nih.gov.
† Center for Molecular Modeling, Division of Computational Bioscience, Center for Information Technology, National Institutes of Health.
‡ Molecular Imaging Branch, National Institute of Mental Health, National Institutes of Health.
§ National Heart, Lung and Blood Institute, National Institutes of Health.
# National Institute of Chemistry.

10.1021/jp077738o CCC: $40.75
Published on Web 01/30/2008

SCHEME 1: Structures of Benzodiazepines 1−4, Showing Dihedral Angles and Nomenclature

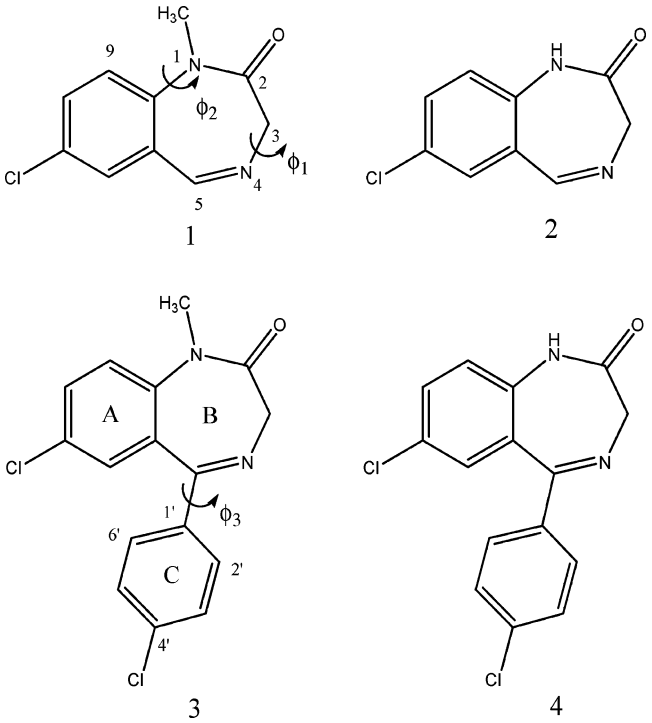

Here, we chose linear interpolation between two minima. The RPATH method adds a harmonic penalty function to the standard force field. This penalty function is proportional to the difference in the root-mean-square distance (rmsd) between the two neighboring structures. In this way, the individual structures on the pathway are kept equidistant in the rms space from their nearest neighbors. This also allows the total length of the path to vary during the simulation, either energy minimization or molecular dynamics.

To assess the applicability of the RPATH method in locating the TS of small yet complex molecules undergoing isomerization without bond breaking, we investigated the inversion of the seven-membered diazepine ring in 1,4-benzodiazepines (BZs) that has been studied both experimentally[11−14] and theoretically.[15−19] A BZ ring appears in several types of bioactive compound and drug and is therefore considered to be a "privileged scaffold" in drug design.[20,21] Best known of these ligands are the BZs acting on central $GABA_A$ receptors (central benzodiazepine receptors; CBR) as anxiolytic and sedative drugs (*e.g.*, diazepam; Valium).[22] Certain derivatives of diazepam, such as the 4′-chloro derivative preferentially bind with high affinity[23] not to CBR but to another distinctly different binding site, the peripheral benzodiazepine receptor (PBR),[24] recently named the translocator 18 kDa protein.[25] PBR has become a promising drug target[26] and also a subject for molecular imaging *in vivo*,[27] primarily of inflammation because of PBR overexpression in activated microglia under several inflammatory conditions.[28] Experimental and computational studies of the conformational dynamics in BZs may have intrinsic value for understanding their important bioactivities. For example, BZs are known to exert their agonist effects at CBR by inducing a conformational change in the receptor.[29] As previously pointed out,[16] the possibility that ring inversion in these drugs plays some role in inducing receptor conformational changes provides impetus for acquiring a deeper and more accurate understanding of these inversion processes.

SCHEME 2: Structures of M and P Conformers of Benzodiazepines Where R^1 Is H or CH_3, and R^2 Is H or *p*-Cl−C_6H_4

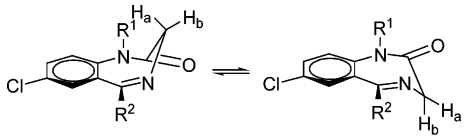

The BZs (**1**−**4** of Scheme 1) studied herein do not have a formal chiral center. Nevertheless, the inversion of the C3 methylene group of the B ring gives rise to two boat conformers that are enantiomers (Scheme 2); by convention, the isoenergetic minimum conformers with a negative and positive value of the dihedral angle C2−C3−N4−C5 (ϕ_1, see Scheme 1) are designated as conformers M and P, respectively.[15] CBR recognize a single enantiomer (designated R or P).[30,31] Previous theoretical work on the inversion of diazepam was performed at the level of "density functional theory" (DFT) only.[15,16]

In the present work, both RPATH and scan methods were used to construct the PES for the inversion of BZs **1**−**4**. Two model compounds **1** and **2** and two more elaborate compounds, namely the PBR ligand Ro5-4864 (**3**) and its N^1-desmethyl analog, Ro5-2752 (**4**) were studied to reveal the effects of N^1-methyl and 5-(4′-chlorophenyl) groups on the inversion energy barrier and the landscape of the reaction path. Comparing the PES of the inversions of **1**−**4** revealed the advantages of the RPATH method as well as the pitfalls of the scan calculation in locating the TS of BZs, and they are here discussed. The reaction path of **3** from the RPATH calculation was also compared with that from the IRC calculation.

2. Methods

2.1. *Ab Initio* RPATH Calculations. Initially, 15 replicas were constructed by a linear interpolation between the two energy-minimized enantiomeric conformers, M and P, of compounds **1**−**4**. The RPATH method then added a harmonic penalty function to the standard energy to restrain distances between adjacent replicas along the reaction pathway, in the form

$$E_{\mathrm{rms}} = \frac{1}{2}\sum_{i=1}^{N-1} K_{\mathrm{rms}}(R_{i,i+1} - \langle R\rangle)^2 \qquad (1)$$

where N is the number of replicas i along the pathway, K_{rms} is the force constant (set here to 10^3 (kcal/mol)/Å^2), and $R_{i,i+1}$ and $\langle R\rangle$ are rmsd deviations given by

$$R_{i,i+1}{}^2 \sum_{j=1}^{n} w_j = \sum_{j=1}^{n} w_j[(x_j^{(i)} - x_j^{(i+1)})^2 + (y_j^{(i)} - y_j^{(i+1)})^2 + (z_j^{(i)} - z_j^{(i+1)})^2]$$

$$\langle R\rangle = N^{-1}\sum_{i=1}^{N-1} R_{i,i+1}$$

where n is the total number of replicated atoms j with coordinates ($x_j^{(k)}$, $y_j^{(k)}$, $z_j^{(k)}$) in replica k, and w_j is a suitable input-defined parameter. Thus, the penalty function[5] is proportional to the difference in the rmsd between the two neighboring structures. In other words, the individual structures on the pathway are kept equidistant in the rms space from their neighbors. In addition, an angle energy term (eq 2) as previously

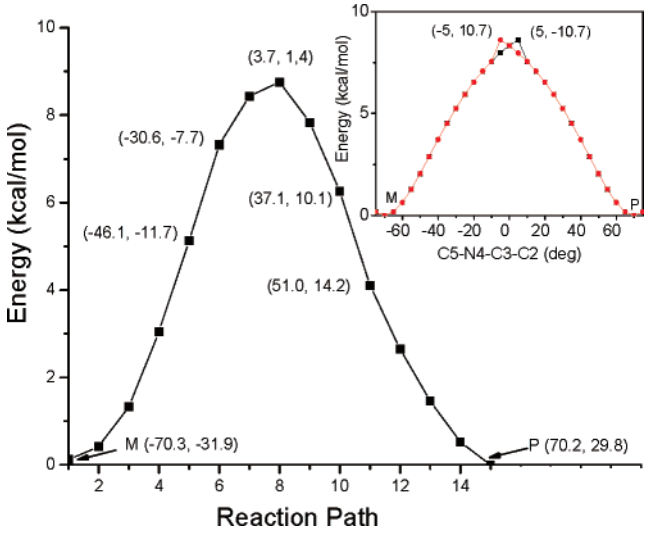

Figure 1. PES for the inversion of benzodiazepine **1** obtained from the RPATH calculation with 15 replicas. During geometry optimization, each replica or frame on the reaction path is kept equidistant in the rms space from their nearest neighbors with a harmonic penalty function. Values in parentheses indicate the dihedral angles C2−C3−N4−C5 (ϕ_1) and CH_3−N1−C10−C9 (ϕ_2); see Scheme 1 for numbering. Inset: PES constructed from both forward and reverse scanning of the ϕ_1 of **1** with an increment of 5°.

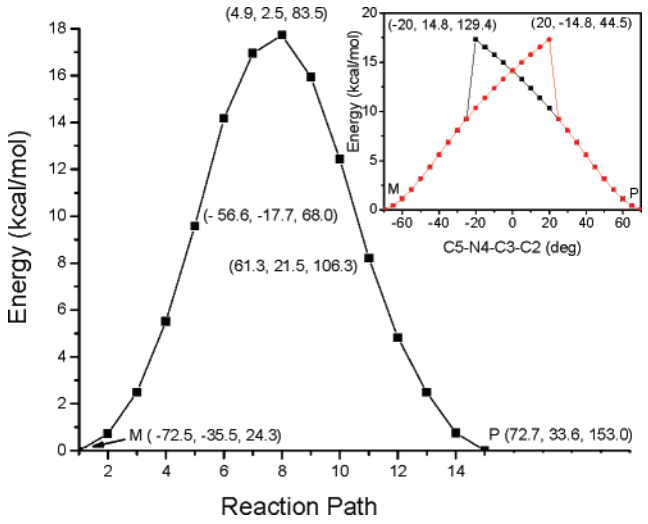

Figure 2. PES for the inversion of compound **3** obtained from the RPATH calculation with 15 replicas. Values in parentheses represent the dihedral angles ϕ_1, ϕ_2, and C6′−C1′−C5−N4 (ϕ_3); see Scheme 1 for numbering. Inset: PES constructed from both forward and reverse scanning of the ϕ_1 of **3**.

defined,[5] was included to prevent merging between the adjacent points (force constants K_{angle}= 100 and cos max = 0.95).

$$E_{angle} = \frac{1}{2}\sum_{i=1}^{N-1} K_{angle}((R^2_{i,i+2} - R^2_{i,i+1} - R^2_{i+1,i+2})/(2R_{i,i+1}R_{i+1,i+2}) - \cos\,\max)^2 \quad (2)$$

The average restraint energy shown in eq 1 was less than 0.1 kcal/mol/replica after 100 steps of energy minimization. After an approximate TS was located, the calculations were further expanded to 61 replicas for compounds **3** and **4**: 30 replicas connecting the stable conformer M to the TS and another 30 replicas linking the TS to P. The *ab initio* program GAMESS was used for all RPATH calculations at the B3LYP/6-31G* level. Further refinement of the TS was carried out with the TS search algorithm using the keywords, opt=(ts, calcfc, noeigentest), as implemented in Gaussian 03 software.[32]

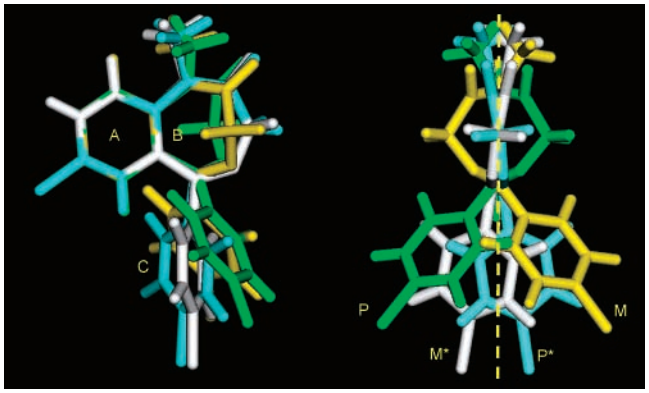

Figure 3. Two perspective views of the superposed energy minimized ground states (M, yellow; P, green) and TSs (M*, white; P*, blue) of **3**. The one on the right-hand side was obtained by rotating the ring A into the plane so that it coincides with the mirror plane indicated by the dotted lines.

TABLE 1: Inversion Energy Barrier of BZs Calculated at the B3LYP/6-31G* Level

	E_a (kcal/mol)	
compound	RPATH[a]	experiment[b]
1	8.6	
2	3.5	
3	17.3	17.6 ± 0.2
4	10.7	12.3 ± 0.3

[a] Values represent the energy difference between the ground state and the fully optimized TS at 0 K without zero point vibration. [b] Determined on compounds without a 4′-chloro substituent.[13]

2.2. *Ab Initio* Calculations. The geometries of the BZ conformers M and P were fully optimized with DFT at the B3LYP/6-31G* level in the gaseous phase. The PES for the inversion process was also calculated by conventional scanning of the dihedral angle ϕ_1 in increments of 5° while optimizing all other geometrical variables. The nature of each TS for compounds **1**−**4** were confirmed by the existence of a single imaginary frequency. In these calculations, thermal and solvent effects were not taken into account in estimating the inversion barriers. The IRC calculations for the inversion of compound **3** were done utilizing 35 steps descending from M* or P* to each of the conformers M and P without mass weighting.

3. Results and Discussion

3.1. Inversions of 1 and 2. The PES of the inversion of the model *N*-methylbenzodiazepine **1** obtained from the RPATH method utilizing 15 replicas is shown in Figure 1. In the conversion of M to P, both the C3 methylene and the N^1-methyl group undergo respective downward and upward inversion with respect to the A ring (Scheme 2), and these two opposite motions are concerted as indicated by the smooth change in both energy and the dihedral angles of ϕ_1 and CH_3−N1−C10−C9 (ϕ_2) given in parentheses in Figure 1. At the highest points of the PES, frame 8, the B ring (ϕ_1 = 3.7°, ϕ_2 = 1.4°) is only slightly distorted from planarity indicating the TS to be symmetrical. The inset of Figure 1 is the PES obtained by the conventional scan calculation by varying the dihedral angle ϕ_1 from −75° to +75° and then by reversing the scan direction from +75° to −75° in increments of 5° while relaxing the rest of the structure. The forward scan has its highest energy at ϕ_1 = 5° and ϕ_2 =

TABLE 2: Dihedral Angles of Compounds 3 and 4 in Both Ground and TSs from RPATH

	M			M*			P*			P		
	ϕ_1	ϕ_2	ϕ_3	ϕ_1	ϕ_2	ϕ_3	ϕ_1	ϕ_2	ϕ_3	ϕ_1	ϕ_2	ϕ_3
3	−72.5	−35.5	24.3	−5.6	−7.0	111.2	5.6	7.0	63.1	72.7	33.6	153.0
4[a]	− 72.6	− 22.4	25.5	−16.4	−4.4	110.3	16.4	4.4	64.4	72.6	22.2	151.5

[a] Dihedral angles from the GAMESS optimized geometries.

−10.7°. A further increase of ϕ_1 to 10° is accompanied by a drop of 1.0 kcal/mol and a rather steep increase in ϕ_2 from −10.7° to +18.0°. This hysteresis in both energetics and geometry results from the hindered rotation of the N^1-methyl group around the N1−C10 bond, which in turn is a consequence of the constraint imposed on the reaction coordinate, ϕ_1. The PES from the RPATH lacks such hysteresis because it minimizes structures at each grid point, thus conveniently diffusing rms restraint forces over all the atoms of the compound during geometry optimization.

Further TS optimization at the highest point on the PES of the two methods with Gaussian 03, resulted in an identical TS geometry where the diazepine ring achieves planarity, conferring a C_s symmetry on the TS, which is in good agreement with the previous finding.[15,16] The RPATH calculation gives the inversion energy barrier as 8.6 kcal/mol for **1** (Table 1).

For the N^1-desmethylbenzodiazepine **2**, both RPATH and scan calculations gave a single reaction path with an inversion barrier of 3.5 kcal/mol without hysteresis. The absence of the rotation of the N^1-methyl group around the N1−C10 bond lowers the inversion energy barrier of **2** by about 5 kcal/mol compared to that of **1**. The subsequent TS optimization at the highest point on the PES obtained from both methods also gave the TS with C_s symmetry.

3.2. Inversion of the PBR Ligand 3. The inversion process of **3** obtained with the RPATH method (Figure 2) is characterized by the rotation of the chlorophenyl group coupled with the movements of the C3 methylene and N^1-methyl groups of the B ring. The similarity of the overall shape of the PES of **3** to that of **1** indicates that the inversion may well occur through a symmetrical TS. Nonetheless, a further TS optimization at the highest PES ($\phi_1 = 4.9°$, $\phi_2 = 2.5°$, $\phi_3 = 83.5°$) resulted in the asymmetrical TS, P* ($\phi_1 = 5.6°$, $\phi_2 = 7.0°$, $\phi_3 = 63.1°$), accompanied by an energy gain of 0.3 kcal/mol. Regardless of the starting geometry chosen near the highest-energy region, we were only able to obtain P*, even after increasing the number of grid points between frames 7 and 10 of Figure 2. This can be attributed to the preference of the TS optimization process with Gaussian 03 at the DFT level for P* over M*. Accordingly, the M* ($\phi_1 = -5.6°$, $\phi_2 = -7.0°$, $\phi_3 = 111.2°$) geometry was obtained by inverting the coordinates of the P* structure (see Figure 3). Note that ϕ_3 is defined as the dihedral angle C6′−C1′−C5−N4 (*e.g.*, 63.1° of P* in Table 2) that is equivalent to the dihedral C2′−C1′−C5−N4 (−111.2°).

The inset of Figure 2 is the PES of the inversion of **3** constructed with the scan method. Both the forward and reverse scans of the reaction coordinate, ϕ_1, are characterized by a sizable hysteresis in energy as well as in geometry at the high-energy region. Apparently, the presence of a 5-(4′-chlorophenyl) group, makes the effect of the constraint imposed on ϕ_1 more strongly felt in both geometry and energetics than in compound **1**. The TS optimization of **3** at the two highest-energy points resulted in the enantiomers M* and P*, as previously pointed out.[15,16]

Utilizing the TS geometry of M* and P* (Figure 3), two reaction paths were then constructed by expanding grid points from 15 to 61: one path connecting the M to P via M* and the other path connecting M to P via P*. These two paths provide more details on the dynamics of the BZ inversion process than hitherto known. The inversion of M to P involves a concerted rearrangement of nuclei and electron redistribution that is manifested in the paths displayed in Figure 4a in terms of the variation of the three dihedral angles (ϕ_1, ϕ_2, and ϕ_3); the two asymmetric paths (M−M*−P and M−P*−P) are symmetric by inversion. Figure 4a shows how the rotation of the chlorophenyl group is synchronized with the inversion of the B ring. When the inversion of **3** takes the M−M*−P path, a significant change in ϕ_3 is observed between the ground state M ($\phi_3 = 24.3°$) and the TS M* ($\phi_3 = 111.2°$). After the TS is passed, a relatively small change of ϕ_3 is seen until the formation of the enantiomer P ($\phi_3 = 153.0°$). This rotation of the chlorophenyl

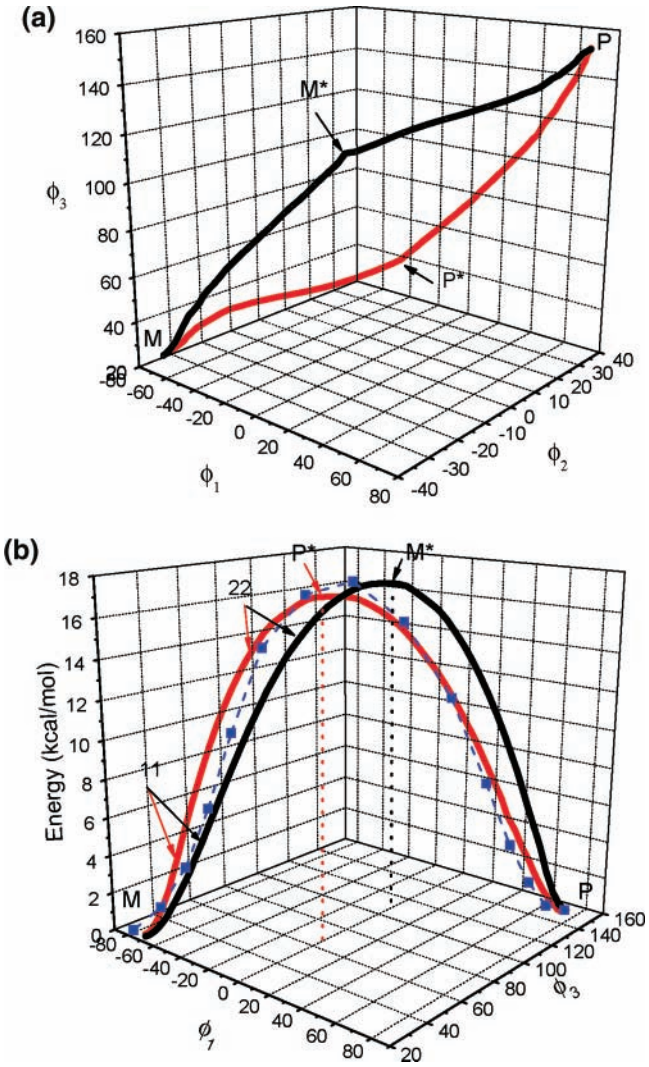

Figure 4. (a) Conversion of the conformer M into P in terms of three dihedral angles (ϕ_1, ϕ_2, and ϕ_3). Two asymmetric paths, M−M*−P and M−P*−P, are symmetrical by inversion. (b) Energetics of the inversion of **3** as a function of ϕ_1 and ϕ_3. Arrows in red and black indicate the frame number on the respective path of M−P*−P and M−M*−P. Dotted lines in red and black depict the position of P* and M*, respectively, in the space of ϕ_1 and ϕ_3.

group is also closely correlated with the inversion of the B ring characterized by ϕ_1 and ϕ_2; both dihedral angles of the conformer M ($\phi_1 = -72.5°$, $\phi_2 = -35.5°$) vary with a small rate of increase until reaching M* ($\phi_1 = -5.6°$, $\phi_2 = -7.0°$), and then with a relatively large increase to P ($\phi_1 = 72.7°$, $\phi_2 = 33.6°$). When the inversion takes the path of M−P*−P, the rates of the chlorophenyl group rotation and the B ring inversion are completely reversed. For example, the ϕ_3 of the conformer M increases from 24.3° to 63.1° up to the P* and then to 153.0° until the inversion is complete. Notably, at the M* and P*, the values of ϕ_1 and ϕ_2 differ by 11.2° and 14°, respectively, as compared to 48.1° for ϕ_3, thus reflecting the larger conformational change of the chlorophenyl group to accommodate the more conformationally restricted seven-membered ring.

Figure 4b illustrates the energetics of the inversion of **3** as a function of ϕ_1 and ϕ_3 showing the two reaction paths going through the M* and P* with an equal energy barrier of 17.3 kcal/mol. The dashed line shown between the two paths is the one taken from the 15 replicas in Figure 2. Because the geometry optimization at each grid point was carried out on the interpolated geometry of M and P with the rms constraint, each point on this dashed path represents the average geometry of particular intermediates of M and P. This quasi-symmetrical path was broken into the two asymmetrical ones when M* and P* were utilized in mapping the inversion, mainly due to the energy difference arising from the rotation of the chlorophenyl ring. For example, frame 11 of the M−P*−P path ($\phi_1 = -64.9°$, $\phi_3 = 37.2°$) is 0.46 kcal/mol more stable than that of the M−M*−P path ($\phi_1 = -64.5°$, $\phi_3 = 49.9°$), and the energy difference becomes smaller at frame 22 (0.23 kcal/mol) and then zero at the TS (frame 31).

3.3. Symmetrical TS. The quasi-symmetrical path shown in Figure 4b together with a small structural difference between the M* and P* suggests that the inversion of **3** can also proceed via a symmetrical TS. A subsequent geometry optimization with C_s symmetry by both Gaussian 03 and GAMESS located the symmetrical TS, which had not been reported before. This newly found TS with C_s symmetry is 0.10 kcal/mol less stable than the asymmetrical M* or P* and has two negative imaginary frequencies; one is related mainly to the B ring puckering (−68.6 cm^{-1}, Figure 5a), and the other to the internal rotation of the chlorophenyl group (−11.9 cm^{-1}, Figure 5b). These two imaginary frequencies further suggest that the inversion of **3** involves multiple TSs that are related by symmetry as in the case of the dissociation of formaldehyde (H_2CO) into H_2 and CO where two nonplanar TSs can be merged into one planar TS.[33] In other words, a path connecting the symmetrical TS to the asymmetrical M* and P* states would enable the inversion via a crossed path such as M−P*-symmetrical TS−P or M−P*-symmetrical TS−M*−P, the latter encompassing the microscopic inversion of the asymmetrical TSs. The RPATH calculation, utilizing 43 replicas between M* and P*, did indeed find such a path with a symmetrical TS, thus demonstrating that the inversion paths of **3** can readily cross from one to the other. The symmetrical TS obtained from the RPATH calculation is essentially identical to that obtained from Gaussian 03 or GAMESS, as shown in Table 3; the energy difference between the RPATH and GAMESS results is 0.0027 kcal/mol. It is noteworthy that the TS with C_s symmetry cannot be obtained with standard TS optimizers in Gaussian 03 or GAMESS without imposing a symmetry constraint whereas the RPATH naturally yields such TS via focusing.

The TS with or without C_s symmetry has intriguing structural features that warrant further examination. To make a meaningful

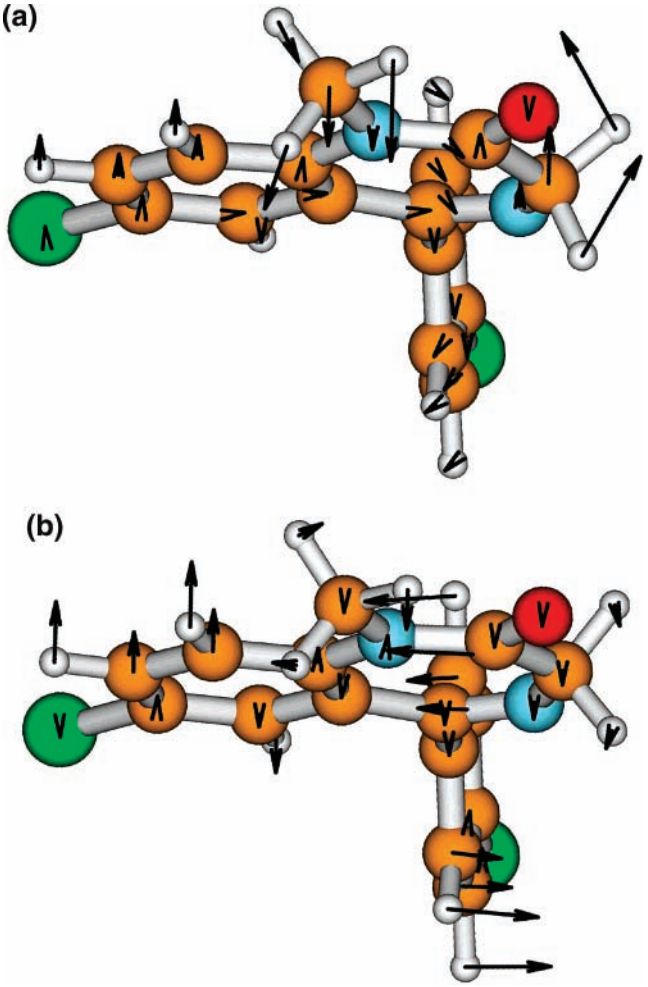

Figure 5. (a) Imaginary vibrational motion of the diazepine ring associated with the N^1-methyl and C3 methylene of the symmetrical TS of **3**. (b) Imaginary torsional vibrational motion of the 5-(4′-chlorophenyl) group of the symmetrical TS of **3**.

structural comparison, it is necessary to focus on the bond distances and angles in Table 3 calculated with the same software (Gaussian 03). First, the C ring of the conformer P, the asymmetrical P*, and the symmetrical TS all deviate from planarity with respect to the plane containing the C1′−C5 bond, as indicated by their respective dihedral angles (177.3°, 174.4°, 175.9°) of C2′−C6′−C1′−C5. This distortion is likely to be a consequence of the steric repulsion between the rings of A and C and is the reason that the dihedral angle C6′−C1′−C5−N4 of the symmetrical TS is 87.9° rather than 90°. Of the two TSs, the symmetrical TS has a smaller distortion because the near orthogonality of the C ring to the B ring attenuates the steric repulsion. Second, the intra-ring bond distances of the B ring of both TSs, such as those of N1−C2, C2−C3, C3−N4, and C10−N1, are quite comparable or slightly different (≤0.0006 Å). Though still small, the difference in the bond distances N4−C5 and C5−C1′ between the two TSs is noteworthy. As compared to the case for asymmetrical P*, the N4−C5 distance of the symmetrical TS is shorter by 0.0014 Å, an indication of a little better overlap of π-electrons over the N4 and C5 atoms due to the flat B ring. On the contrary, the inter-ring bond distance, C5−C1′, of the symmetrical TS is longer by 0.0018 and 0.0238 Å than that of the respective P* and the conformer P: a consequence of unfavorable overlap of π-electron clouds over the C5 and C1′ atoms because the C ring of the symmetrical TS is almost perpendicular to the B ring, as shown by the

TABLE 3: Calculated Distances (Å) and Angles (deg) of the Ground State and TS of 3

	P	P*	symmetrical TS		
parameter	RPATH	Gaussian 03	Gaussian 03	GAMESS	RPATH[a]
N1−C2	1.3951	1.3946	1.3952	1.3950	1.3941
C2−C3	1.5282	1.5275	1.5280	1.5289	1.5286
C3−N4	1.4544	1.4252	1.4253	1.4249	1.4248
N4−C5	1.2862	1.2739	1.2725	1.2725	1.2728
C10−N1	1.4154	1.4218	1.4224	1.4225	1.4228
C10−C11	1.4167	1.4327	1.4327	1.4339	1.4345
C11−C5	1.4921	1.4981	1.4976	1.4979	1.4982
C5−C1′	1.4933	1.5153	1.5171	1.5166	1.5172
C5−N4−C3−C2	72.7	5.6	0.0	0.0	0.0
C6′−C1′−C5−N4	153.0	63.1	87.9	87.6	87.4
C2′−C6′−C1′−C5	177.3	174.4	175.9	175.4	174.9

[a] Obtained from frame 21 having the highest energy among 43 replicas between M* and P*.

TABLE 4: Low Vibrational Frequencies of 3

transition state	frequency (cm^{-1})	mode[a]
asymmetrical (P*)	16.4	C═O out of plane
	28.3	C ring twisting
	40.1	C ring wagging
	83.6	symmetrical N−CH_3 and CH_2 out of plane
symmetrical	19.4	C═O out of plane, A″
	36.8	A ring deformation, A″
	37.3	C ring wagging, A′
	84.2	symmetrical N−CH_3 and CH_2 out of plane, A″

[a] A′ and A″ represent respectively the symmetric and antisymmetric vibration with respect to the σ_h plane.

dihedral angle C6′−C1′−C5−N4 (87.9° vs 63.1° of P* and 153.0° of P). This structural comparison suggests that the geometry relaxation from the symmetrical TS to the asymmetrical TS is subtly manifested by the difference in both the C ring distortion and the bond distances N4−C5 and C5−C1′.

In the phenomenon known as Peierls distortion,[34] a vibronic coupling is responsible for the symmetry breaking of the ground state as observed in polyacetylene[35,36] and cyclobutadiene[37] whose bond-length alternating structures are more stable than their respective equal bond-length structures. By analogy, the C_s symmetry of the benzodiazepine TS can be broken into the more stable enantiomeric M* and P* by a coupled motion of the puckering of the diazepine ring (Figure 5a) to the torsional vibration of the chlorophenyl group (Figure 5b). This notion is strengthened by the existence of a number of low-energy vibrational modes ranging from 20 to 100 cm^{-1} associated with both TSs, as listed in Table 4. Similarly, a coupling between the vibrational mode of NO_2 and the internal rotation of CF_3 leading to geometry relaxation (*i.e.*, a dihedral angle of 1.4° between the plane of NO_2 and that containing the C−N bond) was reported for a small molecule, CF_3NO_2.[38,39] In that study, the calculated energy difference between the eclipsed and the staggered CF_3NO_2 at the MP2/6-311G* level was about 0.1 kcal/mol or 40 cm^{-1} and is quite comparable to the energy difference between the TSs of **3**. Our vibrational frequency calculation at the B3LYP/6-31G* level further identified that the staggered CF_3NO_2 has the TS geometry, suggesting that a vibrational−rotatonal coupling resulting in the rearrangement of nuclei and electron distribution can occur at the TS of both small and complex molecules.

3.4. RPATH vs IRC. Figure 6 illustrates the inversion of **3** obtained from the IRC calculation in terms of ϕ_1 and ϕ_3. Both M−P*−P and M−M*−P have a rather straight path connecting the conformer M to P. Besides, the M−M*−P path is not

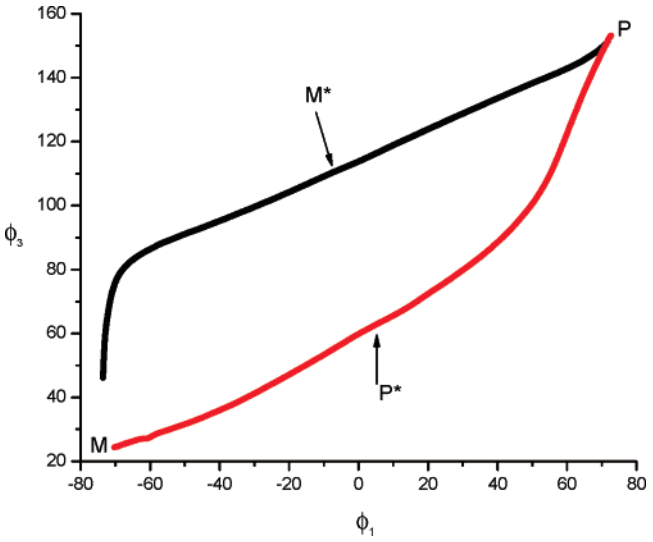

Figure 6. Inversion of **3** in terms of ϕ_1 and ϕ_3 constructed from the IRC calculation.

SCHEME 3: Structure of *trans*-Geldanamycin[a]

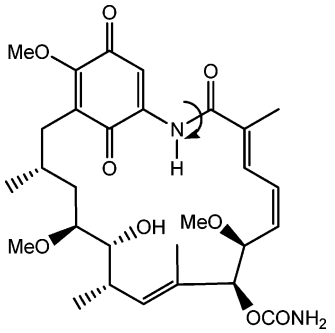

[a] The arrow indicates the amide bond that undergoes *trans*−*cis* isomerization.

symmetrical with the M−P*−P path by inversion as in the case of the RPATH calculations. This is likely to arise from the harmonic character of the normal mode constraint utilized in the IRC method. The RPATH method is not limited by such harmonic approximation and thus better approximates the PES of the inversion of BZs

3.5. Inversion of the *N*-Desmethyl Compound 4. A very similar PES as shown in Figure 4b, with an energy barrier of 10.7 kcal/mol, was obtained for the *N*-desmethyl ligand **4** with the RPATH calculation. The absence of the N^1-methyl group lowers the energy barrier by about 7 kcal/mol with respect to that of **3**, and the asymmetrical M* and P* are 0.07 kcal/mol more stable than the TS with the C_s symmetry. The symmetrical

TS of **4** has one imaginary vibrational frequency (-56 cm^{-1}) mainly associated with ring puckering as shown in Figure 5a.

4. Conclusions

The binding of bioactive ligands to receptors can be accompanied by conformational alterations in both ligand and receptor. A general practical method for exploring conformational pathways including transition points in complex molecules is needed. Embedding the RPATH method in CHARMM with internal access to the major *ab initio* quantum chemical codes provides such a method. RPATH had been tested for mapping a reaction path at an enzyme site, and it is now being tested for the behavior of the TS in bioactive ligands. The importance of the diazepine ring was outlined in the introduction. The present results show that accurate TS behavior for complicated ligands is readily obtained with the RPATH method. The TS of BZs **1**−**4** were successfully located, and the calculated energy barriers for the PBR ligand **3** and its *N*-desmethyl analog **4** were comparable to those experimentally determined for CBR ligands without a 4′-chloro substituent. By further analyzing the conversion of the enantiomeric conformer M into P in both **3** and **4** in torsional space, we discovered that (i) the difference in the rate of the inversion of the diazepine ring and the rotation of the 5-(4′-chlorophenyl) group gives rise to two unsymmetrical paths, (ii) a path connects two asymmetrical TSs of **3** via a symmetrical TS, resulting in multiple inversion paths, (iii) the coupling of the vibrational motion of the diazepine ring and the torsional vibration of the 5-(4′-chlorophenyl) group at the TS stabilizes the asymmetrical TS of **3** and **4** over the TS with C_s symmetry, and (iv) the geometry relaxation of the symmetrical TS of **3** to the asymmetrical TS is manifested by the subtle difference in the C-ring distortion and the bond distances N4−C5 and C5−C1′.

Unlike the traditional scan calculation, which imposes a severe constraint on the reaction coordinate, the RPATH method allows the concerted movement of all atoms, thus avoiding hysteresis in energy and geometry during the inversion of the molecules. In addition, the RPATH does not require *a priori* knowledge of the geometry of the TS of interest, and this provides an advantage for locating the TS of molecules containing many degrees of freedom. For example, the active form of geldanamycin (Scheme 3), an anticancer compound that is recognized by heat shock protein 90, exists in the compact *cis* form whereas the more stable form in solution is in the extended *trans* form.[40] Because geldanamycin has a 16-membered ring with a number of rotatable bonds, other TS searching algorithms may not be practical to approximate the TS of the *trans*−*cis* isomerization of geldanamycin. However, the RPATH method does locate the TSs in the isomerization of geldanamycin (to be published), and thus, it can find a wider application in the study of even complex reaction mechanisms of chemical and biological interest.

Acknowledgment. This research was supported by the Intramural Research Program of the National Institutes of Health, specifically the Center for Information Technology, the National Heart, Lung, and Blood Institute, and the National Institute of Mental Health. M.H. thanks Dr. Bernard R. Brooks and NHLBI for financial support. Y.S.L. thanks Dr. Sergio A. Hassan and Dr. Morris Krauss for many helpful discussions. The quantum chemical study utilized the high-performance computer capabilities of the Helix Systems at the NIH (http://helix.nih.gov) and the PC/LINUX clusters at the Center for Molecular Modeling of the NIH (http://cit.nih.gov).

Note Added after ASAP Publication. This article was released ASAP on January 30, 2008. In section 3.3, paragraph 2, sentence 3 has been revised. The footnote to Table 4 has also been revised. The corrected version posted on January 31, 2008.

References and Notes

(1) Fersht, A. *Enzyme Structure and Mechanism*; W. H. Freeman and Co.: Reading, MA, and San Francisco, 1977; Chapter 10.

(2) Fukui, K. *Acc. Chem. Res.* **1981**, *14*, 363.

(3) Gonzalez, C.; Schlegel, H. B. *J. Chem. Phys.* **1989**, *90*, 2154.

(4) Gonzalez, C.; Schlegel, H. B. *J. Chem. Phys.* **1991**, *95*, 5853.

(5) Woodcock, H. L.; Hodoscek, M.; Sherwood, P.; Lee, Y. S.; Schaefer, H. F., III; Brooks, B. R. *Theor. Chem. Acc.* **2003**, *109*, 140.

(6) Eurenius, K. P.; Chatfield, D. C.; Brooks, B. R.; Hodoscek, M. *Int. J. Quantum Chem.* **1996**, *60*, 1189.

(7) Schmidt, M. W.; Baldridge, K. K.; Boatz, J. A.; Elbert, S. T.; Gordon, M. S.; Jensen, J. H.; Koseki, S.; Matsunaga, N.; Nguyen, K. A.; Su, S.; Windus, T. L.; Dupuis, M.; Montgomery, J. A. *J. Comput. Chem.* **1993**, *14*, 1347.

(8) Woodcock, H. L.; Hodoscek, M.; Gilbert A. T. B.; Gill P. M. W.; Schaefer, H. F., III; Brooks, B. R. *J. Comput. Chem.* **2007**, *28*, 1485.

(9) Guest, M. F.; van Lenthe, J. H.; Kendrick, J.; Sherwood P. (GAMESS-UK is a package of ab initio programs) with contributions from, Amos, R. D.; Buenker, R. J.; van Dam, H.; Dupuis, M.; Handy N. C.; Hillier I. H.; Knowles P. J.; Bonacic-Koutecky, V.; von Niessen, W.; Harrison R. J.; Rendell A. P.; Saunders V. R.; Schoffel, K.; Stone, A. J.; Tozer, D.

(10) Elber, R.; Karplus, M. *Chem. Phys. Lett.* **1987**, *139*, 375.

(11) Finner, E.; Zeugner, H. Z.; Milkowski, W. *Arch. Pharm.* **1984**, *317*, 369.

(12) Finner, E.; Zeugner, H. Z.; Milkowski, W. *Arch. Pharm.* **1984**, *317*, 1050.

(13) Linscheid, P.; Lehn, J.-M. *Bull. Chim. Soc. Fr.* **1967**, 992.

(14) Gilman, N. W.; Rosen, P.; Earley, J. V.; Cook, C.; Todaro, L. J. *J. Am. Chem. Soc.* **1990**, *112*, 3969.

(15) Paizs, B.; Simonyi, M. *Chirality* **1999**, *11*, 651.

(16) Lam, P. C. H.; Carlier, P. R. *J. Org. Chem.* **2005**, *70*, 1530.

(17) Loew, G. H.; Nienow, J. R.; Poulsen, M. *Mol. Pharmacol.* **1984**, *26*, 19.

(18) Messinger, J.; Buss, V. *J. Org. Chem.* **1992**, *57*, 3320.

(19) Gilman, N. W.; Rosen, P.; Earley, J. V.; Cook, C.; Blount, J. F.; Todaro, L. J. *J. Org. Chem.* **1993**, *5*8, 3285.

(20) Ellman, J. A. *Acc. Chem. Res.* **1996**, *29*, 132.

(21) Nakinishi, H.; Kahn, M. In *The Practice of Medicinal Chemistry*, 2nd ed.; Wermuth, D. G., Ed.; Academic Press and Elsevier: Amsterdam, 2003; Chapter 29.

(22) Sternbach, L. H. *J. Med. Chem.* **1979**, *22*, 1.

(23) Bourguignon, J.-J. In *Peripheral Benzodiazepine Receptors*; Academic Press Ltd.: New York, 1993; Chapter 3.

(24) Braestrup, C.; Papadopoulos, V.; Baraldi, M.; Guilarte, T. R.; Knudsen, T. B.; Lacapere, J. J.; Lindemann, P.; Norenberg, M. D. Albrechtsen, R.; Squires, R. F. *Nature* **1977**, *269*, 702.

(25) Papadopoulos, V.; Baradli, M.; Guilarte, T. R.; Knudsen, T. B.; Lacapere, J. J.; Lindemann, P.; Norenburg, M. D.; Nutt, D.; Weizman, A.; Zhang, M. R.; Gavish, M. *Trends Pharmacol. Sci.* **2006**, *27*, 402.

(26) Galiegue, S.; Tinel, N.; Casellas, P. *Curr. Med. Chem.* **200**3, *10*, 1563.

(27) Venneti, S.; Lopresti, B. J.; Wiley, C. A. *Prog. Neurobiol.* **2006**, *80*, 308.

(28) Benavides, J.; Fage, D.; Carter, C.; Scatton, B. *Brain Res.* **1997**, *421*, 167.

(29) Williams, D. B.; Akabas, M. H. *Mol. Phamrmacol.* **2000**, 58, 1129.

(30) Blount, J. F.; Fryer, R. I.; Gilman, N. W.; Todaro, L. J. *Mol. Pharmacol.* **1983**, *24*, 425.

(31) Simonyi, M.; Maksay, G.; Kovács, I.; Tegyey, Z.; Párkányi, L.; Kálmán, A.; Ötvös, L. *Bioorg. Chem.* **1990**, *18*, 1.

(32) Frisch, M. J.; Trucks, G. W.; Schlegel, H. B.; Scuseria, G. E.; Robb, M. A.; Cheeseman, J. R.; Montgomery, J. A., Jr.; Vreven, T.; Kudin, K. N.; Burant, J. C.; Millam, J. M.; Iyengar, S. S.; Tomasi, J.; Barone, V.; Mennucci, B.; Cossi, M.; Scalmani, G.; Rega, N.; Petersson, G. A.; Nakatsuji, H.; Hada, M.; Ehara, M.; Toyota, K.; Fukuda, R.; Hasegawa, J.; Ishida, M.; Nakajima, T.; Honda, Y.; Kitao, O.; Nakai, H.; Klene, M.; Li, X.; Knox, J. E.; Hratchian, H. P.; Cross, J. B.; Adamo, C.; Jaramillo, J.; Gomperts, R.; Stratmann, R. E.; Yazyev, O.; Austin, A. J.; Cammi, R.; Pomelli, C.; Ochterski, J. W.; Ayala, P. Y.; Morokuma, K.; Voth, G. A.; Salvador, P.; Dannenberg, J. J.; Zakrzewski, V. G.; Dapprich, S.; Daniels, A. D.; Strain, M. C.; Farkas, O.; Malick, D. K.; Rabuck, A. D.;

Raghavachari, K.; Foresman, J. B.; Ortiz, J. V.; Cui, Q.; Baboul, A. G.; Clifford, S.; Cioslowski, J.; Stefanov, B. B.; Liu, G.; Liashenko, A.; Piskorz, P.; Komaromi, I.; Martin, R. L.; Fox, D. J.; Keith, T.; Al-Laham, M. A.; Peng, C. Y.; Nanayakkara, A.; Challacombe, M.; Gill, P. M. W.; Johnson, B.; Chen, W.; Wong, M. W.; Gonzalez, C.; Pople, J. A. *Gaussian 03*, revision C.02; Gaussian, Inc.: Wallingford, CT, 2004.

(33) Miller, W. H. *J. Phys. Chem*. **1983**, *87*, 21.

(34) Longuet-Higgins, H. C. *Proc. R. Soc. London Ser. A* **1959**, *251*, 172.

(35) Whangbo, M. H.; Hoffmann, R.; Woodward, R. B. *Proc. R. Soc., London Ser. A* **1979**, *366*, 23.

(36) Lee, Y. S.; Kertesz, M. *J. Chem. Phys.* **1988**, *88*, 2609.

(37) Albright, T. A.; Burdett, J. K.; Whangbo, M. H. C. *Orbital Interactions in Chemistry*; John Wiley and Sons, Inc.: New York, 1985; Chapter 12.

(38) Tolles, W. M. *J. Chem. Phys.* **1993**, *99*, 5718.

(39) Stephenson, E. H.; Macdonald, J. N. *J. Mol. Struct*. **1996**, *376*, 39.

(40) Lee, Y. S.; Marcu, M. G.; Neckers, L. *Chem. Biol*. **2004**, *11*, 991.